FULL PAPER

Deep subduction of the Philippine Sea slab and formation of slab window beneath central Japan

Kazuki Miyazaki[1][*] , Junichi Nakajima[1], Nobuaki Suenaga[2] and Shoichi Yoshioka[2,3]

Abstract

The geometry of the Philippine Sea slab (PHS) subducting beneath the Japanese islands has been imaged to 400 km depth beneath the Kyushu and Chugoku regions, whereas the PHS slab geometry beneath the Hokuriku region has only been determined to ~140 km depth, thereby indicating a large east–west asymmetry in the slab subduction. However, geologic evidence suggests that there was symmetrical east–west seafloor spreading along the axis of the Kinan seamount chain when the Shikoku basin was an active spreading center in the PHS plate. This inconsistency suggests that the PHS slab should be present beneath the Hokuriku region. Here we perform P-wave travel-time tomography across central Japan and conduct a two-dimensional plate subduction numerical simulation that reproduces the dual subduction of the PHS and Pacific (PAC) plates to elucidate the PHS slab geometry beneath central Japan. The tomography results reveal a high-velocity anomaly at ~150–250 km depth that extends from Wakasa bay to Noto peninsula and a slab window beneath the Hokuriku region. The numerical simulation results suggest that the PHS slab may have torn when it collided with the PAC slab, with the once leading edge of the PHS slab now present along the upper surface of the PAC slab beneath Noto peninsula. These results indicate that the PHS slab exists at ~250 km depth beneath the Hokuriku region, although it has been torn owing to its collision with the PAC slab, with this tear propagating westward to form a triangular slab window beneath the Hokuriku region.

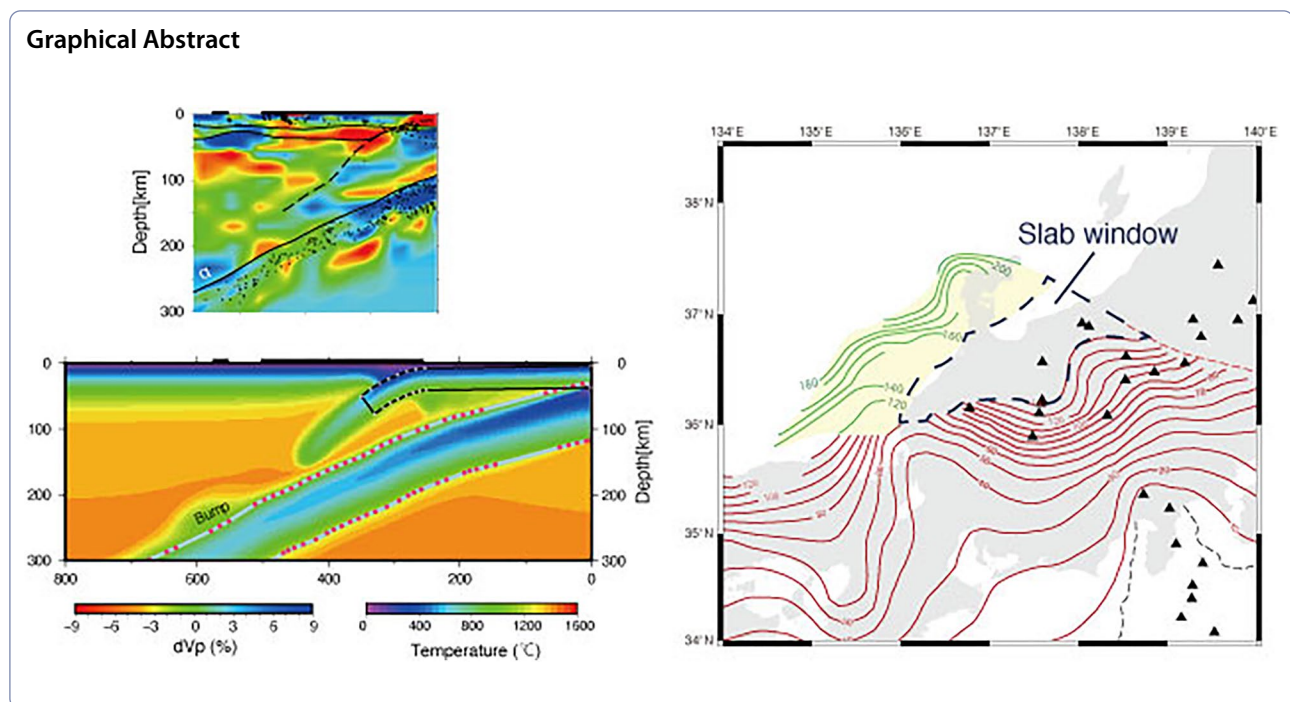**Keywords** Seismic tomography, Numerical simulation, Slab interaction

*Correspondence:
Kazuki Miyazaki
miyazaki.k.ak@m.titech.ac.jp
Full list of author information is available at the end of the article

Miyazaki *et al. Earth, Planets and Space*　(2023) 75:93

Page 2 of 17

Graphical Abstract

Introduction

The Philippine Sea (PHS) plate subducting beneath the central part of southwestern Japan formed at ~ 30–15 Ma via seafloor spreading along the Shikoku basin. This seafloor spreading split an ancient arc into two parts in the almost E–W direction (Fig. 1): the Kyushu–Palau ridge (KPR), which runs from the east of Kyushu to the Palau islands, and Izu–Bonin Mariana (IBM) arc, which is an active arc located along the west of the IBM trench (e.g., Seno and Maruyama 1984; Okino et al. 1994; Sdrolias et al. 2004). After the spreading termination in the Shikoku basin at ~ 15 Ma, the KPR, IBM, and spreading axis of the Shikoku basin (Kinan seamount chain) started to subduct beneath Japanese islands. Although seismic and other geophysical surveys have traced the subduction of the KPR to the central part of Kyushu (Park et al. 2009; Yamamoto et al. 2013; Nakajima 2019), plate reconstruction modeling has suggested that remnants of the subducted KPR may extend as far as Tsushima island (Fig. 1; Cao et al. 2014). The IBM trench corresponds to the eastern limit of the PHS plate, and the eastern limit of the subducted PHS plate is estimated to bend westward after the subduction (Uchida et al. 2009). The Kinan seamount chain, which is the fossil spreading axis of the PHS plate and is currently subducting beneath the Kii channel and the Chugoku region, is considered to be the cause of the anomalously high ^{3}He/^{4}He ratios in the Kinki region (Sano and Nakajima 2008; Sano et al. 2009) and the proposed slab tear beneath the Kii channel (Ide et al. 2010).

The geometry of the PHS slab has been updated by combining recent tomography results (Hirose et al. 2008; Nakajima et al. 2009; Zhao et al. 2012; Huang et al. 2013; Asamori and Zhao 2015; Liu and Zhao 2016; Hua et al. 2018), and indicates that it is subducted to ~ 400 km in the north of Chugoku and west of Kyushu regions. In contrast, tomographic studies have not suggested deep subduction of the PHS slab beneath the Hokuriku region (e.g., Abdelwahed and Zhao 2007; Nakahigashi et al. 2015), where the eastern segment of the fossil spreading axis is subducted,

(See figure on next page.)

Fig. 1 Tectonic setting in southwest Japan. **a** Map of the tectonic setting of the southwestern Japanese islands. Red lines represent the depth contours of the upper surface of the PHS slab. The geometry of the PHS slab (Hirose et al. 2008; Hua et al. 2018) has been determined by integrating the results of various recent seismic analyses (Hirose et al. 2008; Nakajima et al. 2009; Zhao et al. 2012; Huang et al. 2013; Asamori and Zhao 2015; Liu and Zhao 2016; Hua et al. 2018). The iso-depth contours are provided at a 10-km interval for the shallow section (~ 150 km) and a 30-km interval for the deep section (> 150 km). The thin dotted blue lines represent the subducting PAC slab to 250 km depth at every 50-km interval (Nakajima and Hasegawa 2006). The shaded red zone represents the contact zone of the PHS and PAC slabs (Nakajima et al. 2009). Dashed black lines represent trenches and troughs. Bold dashed blue lines represent the locations of the extinct Kinan seamount chain and the Kyushu–Palau ridge. Black triangles represent volcanoes. **b** Location names in the study area (same area as in a) that are mentioned in the text. The inset map shows the location of the study region
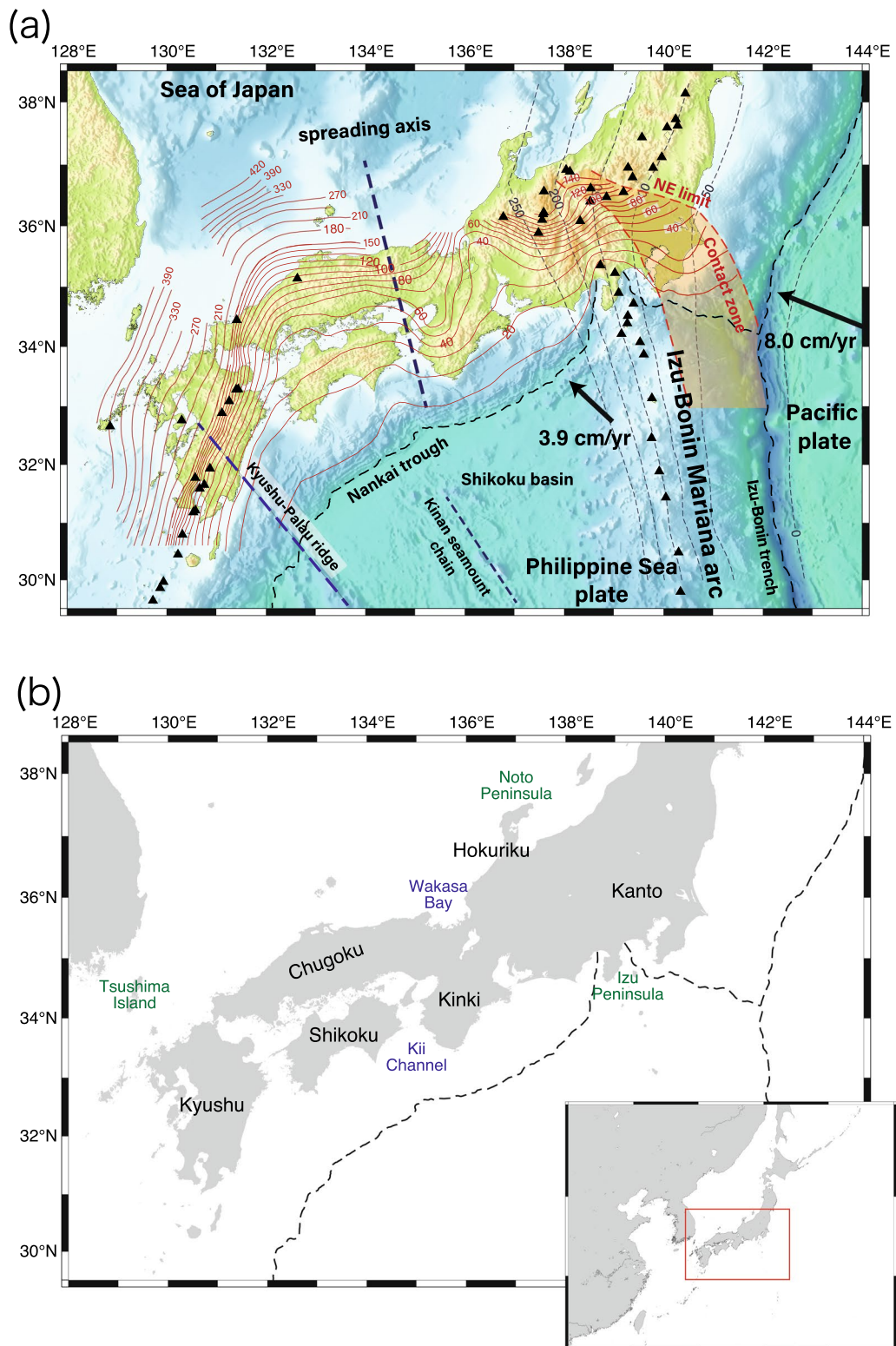
Fig. 1 (See legend on previous page.)

Miyazaki *et al. Earth, Planets and Space*   (2023) 75:93

Page 4 of 17

and the subducted PHS slab has only been determined to ~ 140 km depth. There is therefore a large east–west asymmetry in the depth extent of the PHS slab subduction (Fig. 1a). However, since the fossil spreading axis is almost perpendicular to the Nankai trough, the amount of subduction would be symmetrical in the eastern and western part of the axis if the subduction velocity has not significantly changed along the Nankai trough. This inconsistency indicates that the PHS slab may be hidden at > 150 km depth to the east of the fossil spreading axis (from Wakasa bay to the off the coast of the Hokuriku region). Furthermore, Yamamoto et al. (2009) noted that there may be > 700 km of subducted PHS slab based on a paleogeographic reconstruction of the Proto-Izu arc. The subduction of > 700 km of the PHS slab would place the leading edge of the PHS slab beneath the Sea of Japan and supports the hypothesis that the PHS slab exists at > 150 km depth beneath the Hokuriku region.

One reason for the difficulty in determining the geometry of the subducted PHS slab beneath the Hokuriku region is the influence of the underlying Pacific (PAC) slab. The Japanese islands are located near a trench–trench–trench triple junction, with the PAC plate subducting from the east and the PHS plate subducting from the south. The PAC slab is in contact with the overlying PHS slab beneath Kanto (Fig. 1a), which results in significant deformation of the PHS slab (Ishida 1992; Uchida et al. 2010; Kono et al. 2017) and a complex thermal structure in the mantle and the subducting slabs around the slab contact zone (Iwamori 2000; Hasegawa et al. 2007; Yoshioka et al. 2015; Ji et al. 2016; Wada and He 2017). If the PHS slab is present at deeper depth beneath the Hokuriku region, then the PHS slab would contact the PAC slab at deeper depth than currently considered. It is therefore important to discriminate the location of the PHS slab from that of the underlying PAC slab to precisely determine the geometry of the PHS slab.

Here we perform seismic tomography and a numerical simulation of the subduction of the PHS and PAC plates beneath central Japan to better constrain the PHS slab geometry in this region. Our seismic tomography analysis reveals a high-velocity anomaly down to 250 km depth, which we interpret to be the subducting PHS slab. The tomography result also reveals that a slab window may have formed in the PHS slab beneath the Hokuriku region. Our numerical simulation suggests that the PHS slab may have been torn during its collision with the PAC slab, with the position of this slab tear beneath the Hokuriku region. We propose a new PHS slab geometry beneath central Japan and discuss its history based on the results of our seismic tomography and numerical simulation.

Seismic tomography
Data and method
We applied the tomographic method (Zhao et al. 1992) to P-wave arrival time data and hypocenter locations obtained by the Japan Meteorological Agency (JMA). We first selected the $M \geq 2$ earthquakes that occurred in the study area during the January 1998–March 2018 period. We then revised the earthquake dataset to only include earthquakes that had P-wave arrival times at > 20 stations and focal depths that were smaller than the epicentral distances. The latter criterion ensures that the focal depths of the included earthquakes can be constrained by the arrival-time data at the nearest station. We divided the analysis volume into $0.02° \times 0.02° \times 5$ km boxes and selected the earthquake with the largest number of observations in each box to ensure that the earthquake distribution was as spatially uniform as possible. This resulted in the inclusion of 13,140 earthquakes (Fig. 2) which were characterized by 734,923 P-wave arrival times recorded at 668 stations.

The initial P-wave velocity structure was defined as a simplified one-dimensional velocity structure of the JMA2001 velocity model (Ueno 2002). The upper surfaces of the PAC slab (Nakajima and Hasegawa 2007; Nakajima et al. 2009) and continental Moho and the Conrad discontinuities (Katsumata 2010) were prescribed in the model space. The damping factor was set to 200. The seismic velocities were not obtained at the grid nodes that were sampled by < 1000 ray paths.

The grids were spaced every 0.3 degrees in the horizontal direction and about every 30 km in the depth direction (Fig. 3). Two types of grids were used to calculate the velocity model: one in the crust and mantle above the PAC slab, and the other in the PAC slab. The former grid was placed vertically, and the latter grid was placed in the downward direction perpendicular to the PAC slab surface (Zhao et al. 1992). The initial value of the velocity perturbation in the grid nodes in the PAC slab was assigned to be 5% faster than that of the mantle at the same depth. The root mean square of the residual time decreased from 0.45 to 0.33 s after five iterations.

Results
We performed checkerboard resolution tests (CRTs) to evaluate the sensitivity of the seismic tomography results to the ray coverage. We created a synthetic velocity structure with $\pm 10\%$ velocity perturbation at alternating grid nodes and calculated the synthetic travel-time data for this model using the same hypocenter and station distributions as our observation. We also added random noises with a standard deviation of 0.05 s to the calculated synthetic travel-time data, which corresponds to
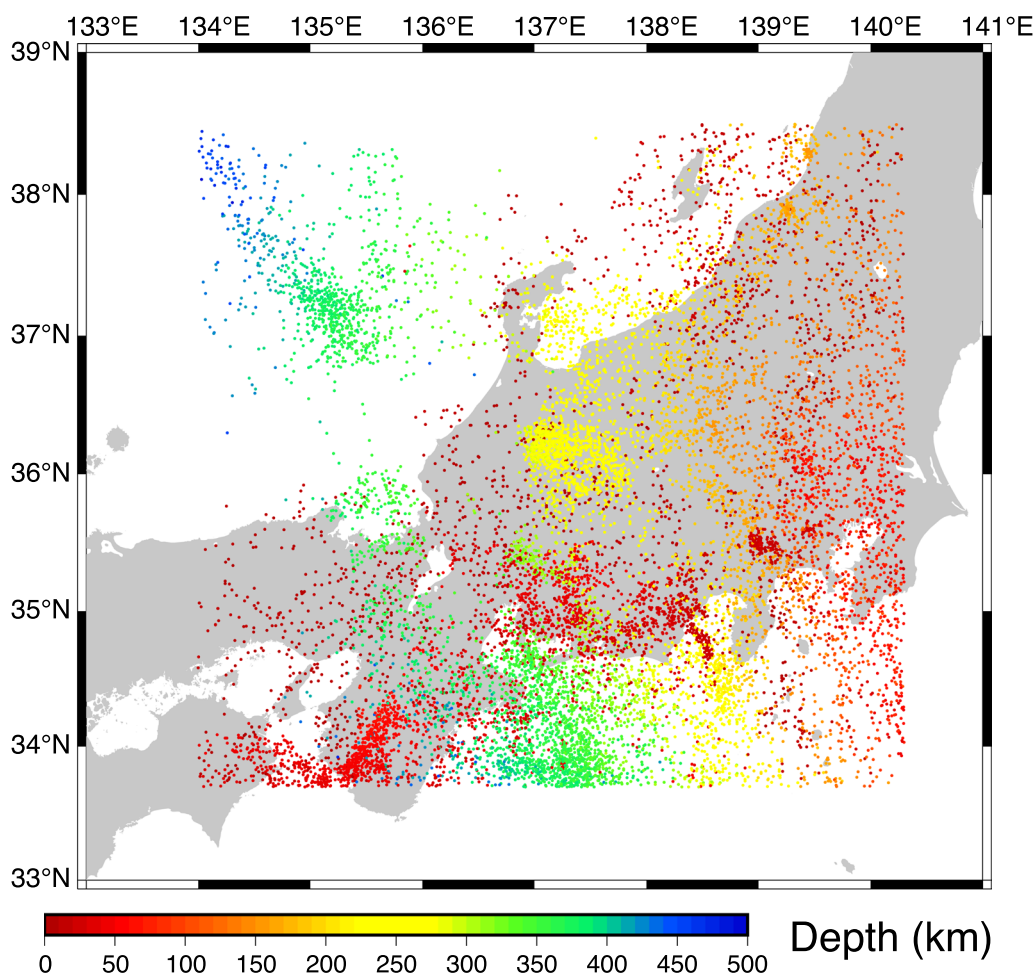
Fig. 2 Regular earthquake distribution used in the tomographic analysis. The $M \geq 2$ earthquakes that were observed by JMA during the January 1998–March 2018 period are used. The earthquakes are color-coded by depth

phase-picking error of the P waves. We then used the generated synthetic travel-time data to perform a tomographic inversion using the initial velocity model with no velocity anomalies. Additional file 1: Fig. S1 shows the CRT results, which demonstrate that the ray coverage of our earthquake dataset is adequate in providing good resolution to ~265 km depth beneath the land area and > 140 km depth beneath the offshore Hokuriku region.

We calculated the recovery rate at each grid node (Nakajima and Hasegawa 2007) using the CRT results, which is defined as the rate of the recovered CRT values for a given velocity perturbation in the synthetic model. A value of + 1 means that the amplitude and polarity are perfectly reproduced. We first calculated the recovery rates at each grid node, and then interpolated the values to estimate the recovery rate at any point in the model space. This study focuses on the deep subduction of the PHS slab beneath Hokuriku region, which means that the

effective recovery of the observed seismic velocity perturbations in this deeper zone is essential. We therefore show the tomography results for areas possessing the recovery rate of > 0.15.

Vertical cross sections of the P-wave velocity structure along seven SSE–NNW-oriented profiles in central Japan are shown in Fig. 4. High-velocity zones exist from south (shallow) to north (deep) at 20–100 km depth along most of the profiles (A1, A2, A4, A5, A6, and A7). These high-velocity zones are interpreted to the PHS slab because these anomalies correspond to the earthquake distribution in the PHS slab and are consistent with the geometry model of the PHS slab (Fig. 1). In particular, the result along profile A7 reveals a continuous high-velocity zone that extends deeper than the previously known geometry of the PHS slab, which suggests that the PHS slab is subducted to ~150 km depth beneath Wakasa bay.

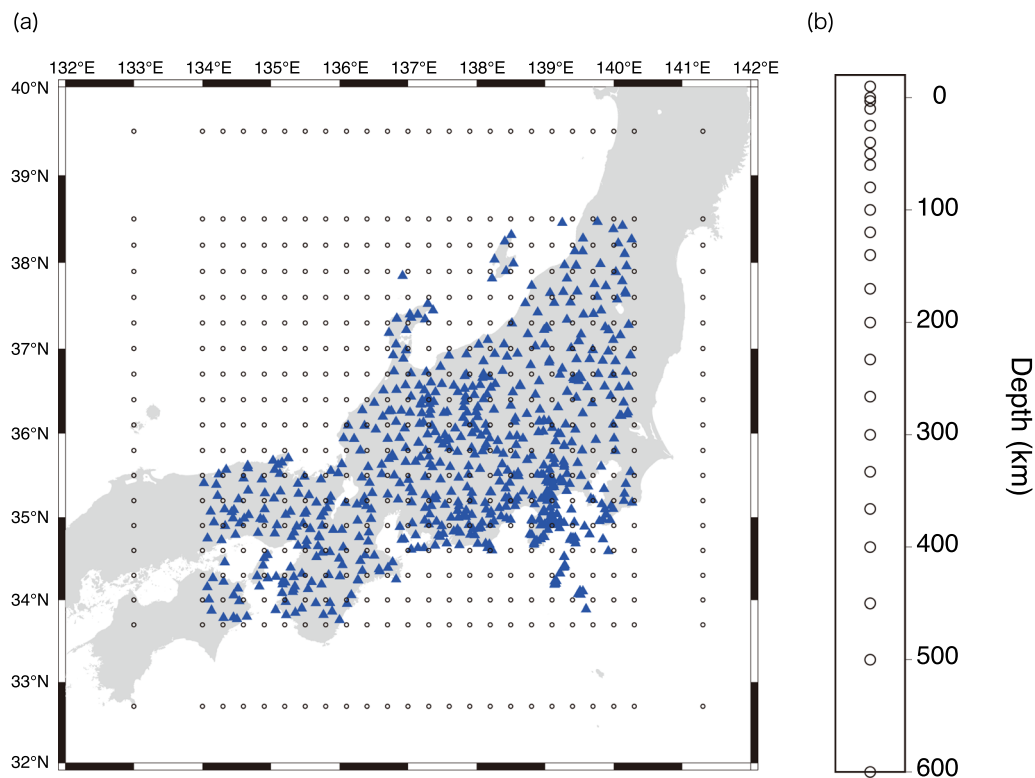A large low-velocity anomaly exists < 50 km depth along profile A3. Previous studies have identified a similar

Fig. 3 Settings used for the seismic tomography. **a** Map view of the seismic stations (blue triangles) and grid nodes (circle), and **b** depth distribution of the calculation grid nodes used in the tomographic analysis

large-scale low-velocity zone at 20–60 km depth beneath the volcanic front around the northern Izu peninsula (Sekiguchi 2001; Nakajima and Hasegawa 2007). Nonvolcanic deep tremors and intermediate-depth earthquakes in the PHS slab are not observed in this region (Arai et al. 2014; Nakajima 2018), and the low-velocity zone in the PHS slab is considered to correspond to the subducting Nishi-Shichito ridge and IBM arc (Nakajima and Hasegawa 2007; Yamamoto et al. 2009; Ishise et al. 2015).

Marked low-velocity zones are imaged beneath active volcanoes along profile A1, A2, A4 and A5, with these low-velocity zones attributed to areas with abundant fluids and/or melt that are associated with the volcanisms. In particular, the low-velocity zone beneath a volcanic belt along profile A4 is continuously imaged down to ~50 km depth. This low-velocity zone has also been imaged by Nakajima and Hasegawa (2007) and is interpreted to be mantle return flow that is induced by the steep subduction of the PHS slab. Such mantle flow enhances the excitation of volcanic activity through the transport of fluids and/or melt from the deep mantle wedge to the continental Moho.

The seismic tomography results reveal a distinct high-velocity anomaly beneath the Noto peninsula that seems to overlie the PAC slab. This is clearly visible in the cross section along profile A4 (Fig. 4) and map viewing (Additional file 1: Fig. S2); we hereafter call this anomaly "segment α". Segment α is characterized differently for the orientation of profiles, as shown in Fig. 5. The directions of profile C1 and C2 are almost the same as the subduction direction of the PHS plate, whereas profile B1 and B2 are perpendicular to the subduction direction. A continuous high-velocity anomaly is observed from shallow depths (~100 km) to segment α along profile B1 and B2 (Fig. 5a, b, respectively). Conversely, the shallow high-velocity anomaly and segment α are separated by a low-velocity anomaly at ~150–200 km depth along profile C1 and C2 (Fig. 5c, d, respectively).

Additional synthetic tests were performed to evaluate the reliability of the observed continuity (profiles B1 and B2) and discontinuity (profiles C1 and C2) between segment α and the shallow high-velocity anomaly. We constructed two synthetic velocity models that characterize the distribution of the high-velocity anomalies related to segment α. The first model prescribes two discontinues rectangular-shaped high-velocity discontinuities (Fig. 6a, e), whereas the second model places an inclined, continuously distributed, high-velocity anomaly at 100–250 km depth (Fig. 6c, g). We generated synthetic arrival-time data for these models using the same hypocenter and
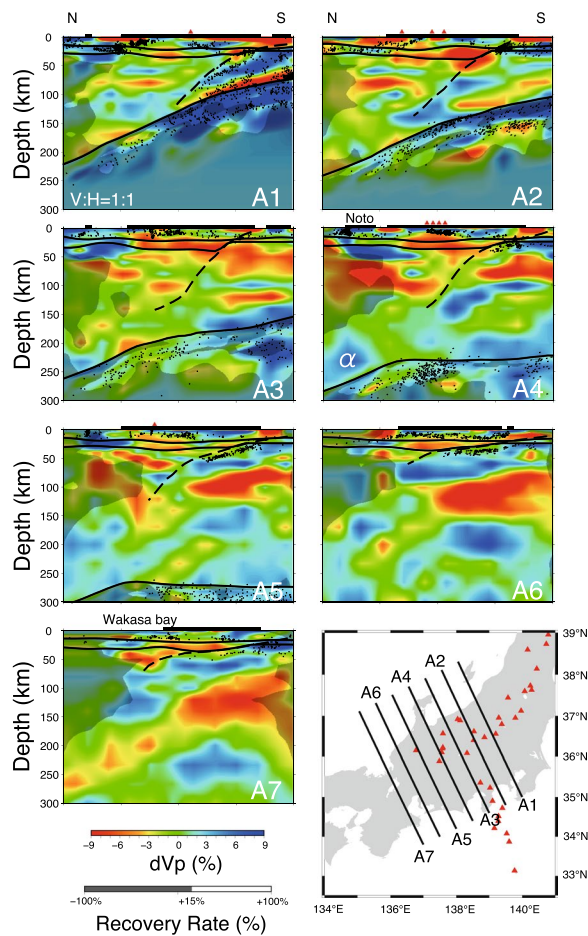
Fig. 4 Vertical cross sections of the seismic structures obtained by the tomographic analysis. Warmer colors indicate lower velocities, and colder colors indicate higher velocities. Each panels show the cross section corresponding to profile A1-A7 in the map. The dotted line in each cross section indicates the subducted PHS slab from the latest PHS slab model (Fig. 1). Solid black lines represent the surfaces of the Conrad (shallowest), Moho, and PAC slab (deepest). Black circles denote the earthquake hypocenters within 10 km of each cross section. Black bars and red triangles in the upper part of each cross section indicate the land areas and volcanoes, respectively. Shaded areas have a recovery rate of < 15%. Locations of the cross sections are shown in the map at the bottom of the figure

station pairs as in the observations, and then performed a tomographic inversion to assess the ability to reproduce the input velocity anomalies. Both models were well reproduced by the synthetic tests (Fig. 6a–d), which suggests that segment α is connected to the shallow high-velocity anomaly along profiles B1 and B2 and separated from the shallow high-velocity anomaly along profiles C1 and C2.

We also performed tomographic inversions with different parameterizations to investigate the influence of the parameter settings on the obtained three-dimensional (3D) velocity images. We used different damping parameter values and grid node configurations during the tests. The parameter values that were used for each test are summarized in Additional file 1: Table S1. Additional file 1: Fig. S3 shows the results of these tomographic calculations for a cross section along profile B1. Although the amplitudes of the velocity anomalies are slightly different, the fundamental features related to segment α are unchanged, thereby confirming that the location of segment α is reliable and robust.

The deep geometry of the PHS slab

The most significant feature in the seismic tomography results is the inclined high-velocity anomaly extending from Wakasa bay to the Noto peninsula (Fig. 5a, b). The results along profiles B1 and B2 show that this high-velocity anomaly is continuous, extending from the segment α to the shallow PHS slab that was defined by previous tomographic studies and hypocenter distributions. We interpret that segment α to be part of the PHS slab, which means that the subducting PHS slab is present beneath the Noto peninsula. We note that previous studies have partly delineated this continuous, inclined, high-velocity anomaly (Abdelwahed and Zhao 2007; Wang and Zhao 2012; Asamori and Zhao 2015; Nakahigashi et al. 2015), however, none of these studies have interpreted the continuous high-velocity anomaly to be the PHS slab to the north of the Hokuriku region.

Figure 7 shows the iso-depth contours of the upper surface of the PHS slab newly delineated from the tomographic analysis in this study (green contours) and those defined in previous studies (red contours). The existence of a deep subducting PHS slab to the north of the Hokuriku region suggests that the hypothesis of symmetric of the PHS slab to the east and west of the Kinan seamount chain is supported at the least 250 km depth. However, we note that the limited resolution of the seismic velocity structure in the Sea of Japan highlights our inability to image the deep subduction of the PHS slab at > 250 km depth.

Our tomographic model revealed the existence of a slab window beneath the Hokuriku region, with our synthetic tests suggesting that this slab window is robust and reliable (Fig. 6). Nakamura et al. (2008) investigated the geochemical components of volcanic rocks from 28 Quaternary volcanoes in central Japan and interpreted that it is unlikely that the PHS slab is being subducted beneath the Hokuriku region because there is no contribution of PHS fluids in the Hokuriku region. The slab window of the PHS slab beneath the Hokuriku region is consistent with these geochemical results.
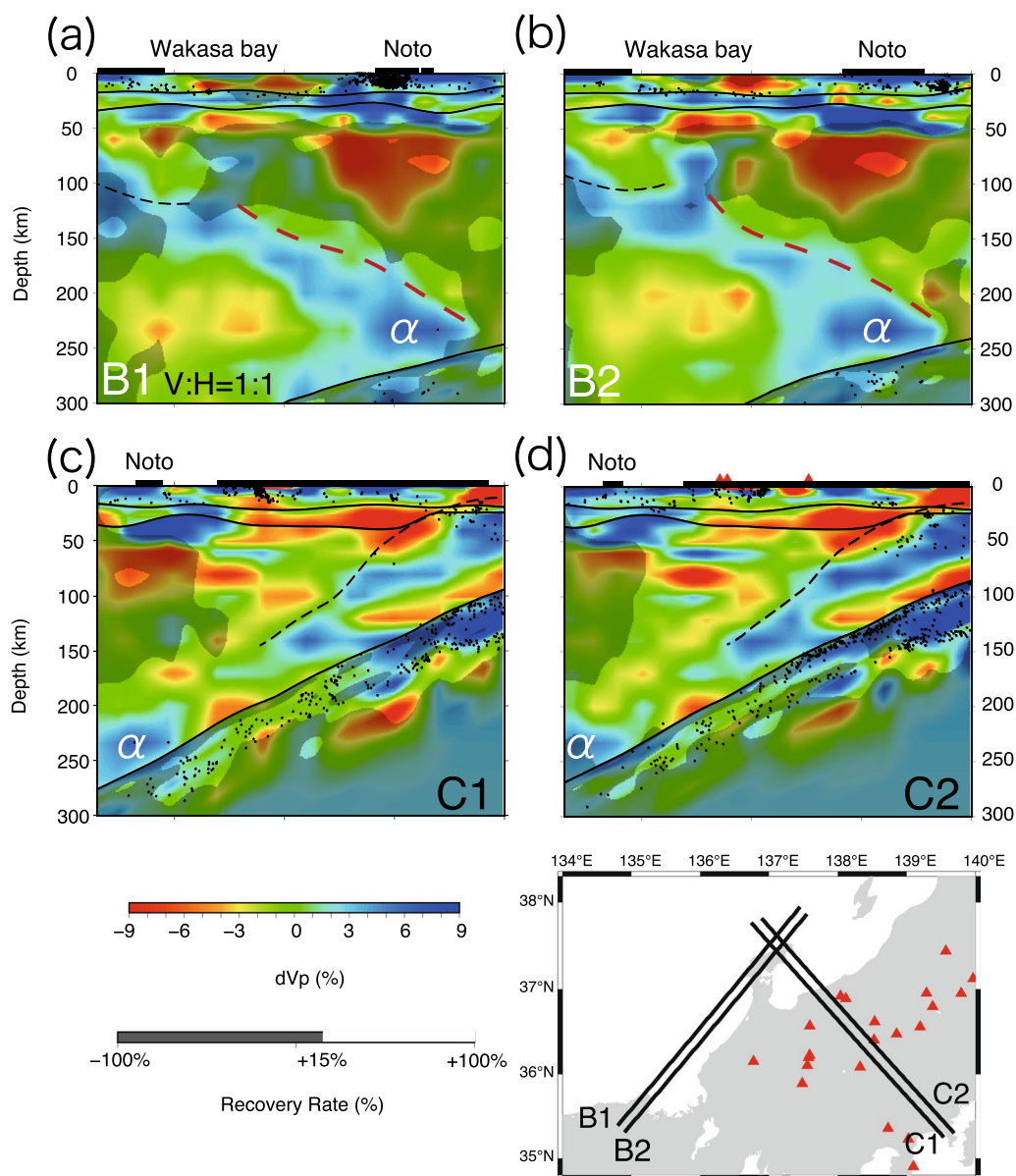
Miyazaki *et al. Earth, Planets and Space*   (2023) 75:93

Page 8 of 17

Fig. 5 Vertical cross sections that highlight the presence of a detectable PHS slab in the tomography results. Each panels show the cross section corresponding to profiles (a) B1, (b) B2, (c) C1 and (d) C2 in the map. All the symbols in the figure are the same as in Fig. 4. The estimated upper boundary of the continuous high-velocity anomaly is shown as a dashed red line

Numerical simulation of plate subduction

The seismic tomography results suggest that the subducted PHS slab extends to ~250 km depth to the north of the Hokuriku region. However, the obtained slab geometry is very complex, with a large slab window present beneath the Hokuriku region. We are unable to discuss the cause of the slab window based solely on the seismic observations, as our seismic tomography results only provide a snapshot of the subsurface structures. Therefore, we performed a two-dimensional (2D) numerical simulation of plate subduction to investigate the physical behavior of the PHS slab and the mechanical interaction between the PHS and PAC slabs beneath central Japan.

Method

We used a 2D box-type model subduction simulation source code that was developed by Yoshioka and Sanshadokoro ([2002]) and partly modified by Torii and Yoshioka ([2007]) and Yoshioka et al. ([2015]). This source code
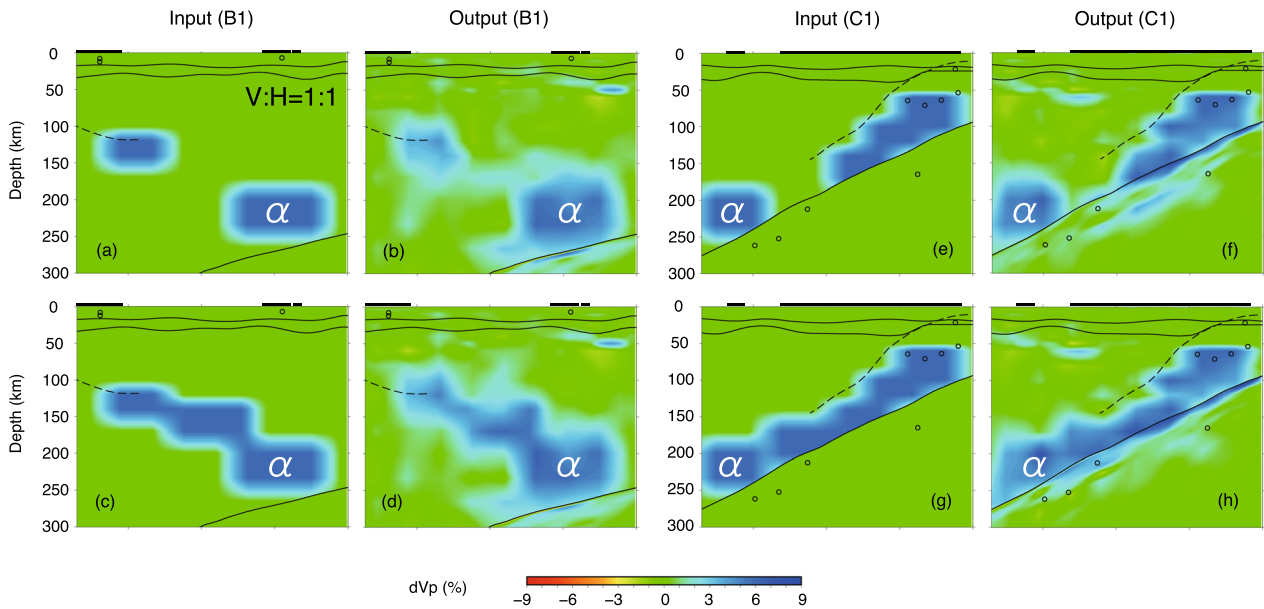
Fig. 6 Synthetic results for four tests. Left panels (**a**, **b**, **c**, and **d**) present the test results along profile B1 in Fig. 5, and right panels (**e**, **f**, **g**, and **h**) present the test results along profile C1 in Fig. 5

solves the momentum and energy equations as a coupled problem with the temperature distribution and stream function for each time step. The momentum equation is written as:

$$\frac{\partial^2}{\partial x \partial z}\left(4\eta\frac{\partial^2\psi}{\partial x \partial z}\right) + \left(\frac{\partial^2}{\partial z^2} - \frac{\partial^2}{\partial x^2}\right)\left[\eta\left(\frac{\partial^2}{\partial z^2} - \frac{\partial^2}{\partial x^2}\right)\psi\right] + \frac{\partial}{\partial x}(\rho_0 g \alpha T) = 0\,,$$

where η is the viscosity, ψ represents the stream function, ρ_0 is the standard density, and g is the acceleration of gravity, α is thermal expansivity, and T is temperature. We take the x-axis from right to left and the z-axis from top to bottom. The energy equation is written as:

$$\rho C_p\left(\frac{\partial T}{\partial t} + \mathbf{v}\cdot\nabla T\right) = k\nabla^2 T + v\rho_0 g \alpha T$$

$$+ 4\eta\left(\frac{\partial^2\psi}{\partial x \partial z}\right)^2 + \eta\left(\frac{\partial^2\psi}{\partial z^2} - \frac{\partial^2\psi}{\partial x^2}\right)^2 + H_0\exp\left(-\frac{z}{10}\right) + \tau\dot{\varepsilon}\,,$$

where $\mathbf{v}$ is the flow velocity vector, ρ is density, C_p is specific heat at constant pressure, t is time, k is thermal conductivity, H_0 is heat generation at the surface, τ is shear stress at the plate interface, and $\dot{\varepsilon}$ is the strain rate at the plate interface.

For the viscosity of the mantle, we use the following equation proposed by Burkett and Billen (2010). In this model, the viscosity η is expressed as composite viscosity of the diffusion creep and dislocation creep of olivine:

$$\eta = \frac{\eta_{\text{diff}}\cdot\eta_{\text{disl}}}{\eta_{\text{diff}} + \eta_{\text{disl}}}\,.$$

η_{diff} and η_{disl} represent the viscosities caused by diffusion creep and dislocation creep, respectively. Under constant pressure, the viscosity is expressed by the following equation:

$$\eta_{\text{diff}}, \eta_{\text{disl}} = \left(\frac{d^q}{AC_{\text{OH}}^r}\right)^{\frac{1}{n}}\dot{\varepsilon}^{\frac{1-n}{n}}\exp\left[\frac{E + P_{\text{lc}}V}{nRT}\right]\,,$$

with

$$\dot{\varepsilon} = \left(\frac{1}{2}\dot{\varepsilon}_{ij}\dot{\varepsilon}_{ij}\right)^{\frac{1}{2}}\,.$$

Here, d is grain size, q is grain-size exponent, r is the water-content exponent, n is stress exponent, A is a coefficient, C_{OH} is water content, E is activation energy,
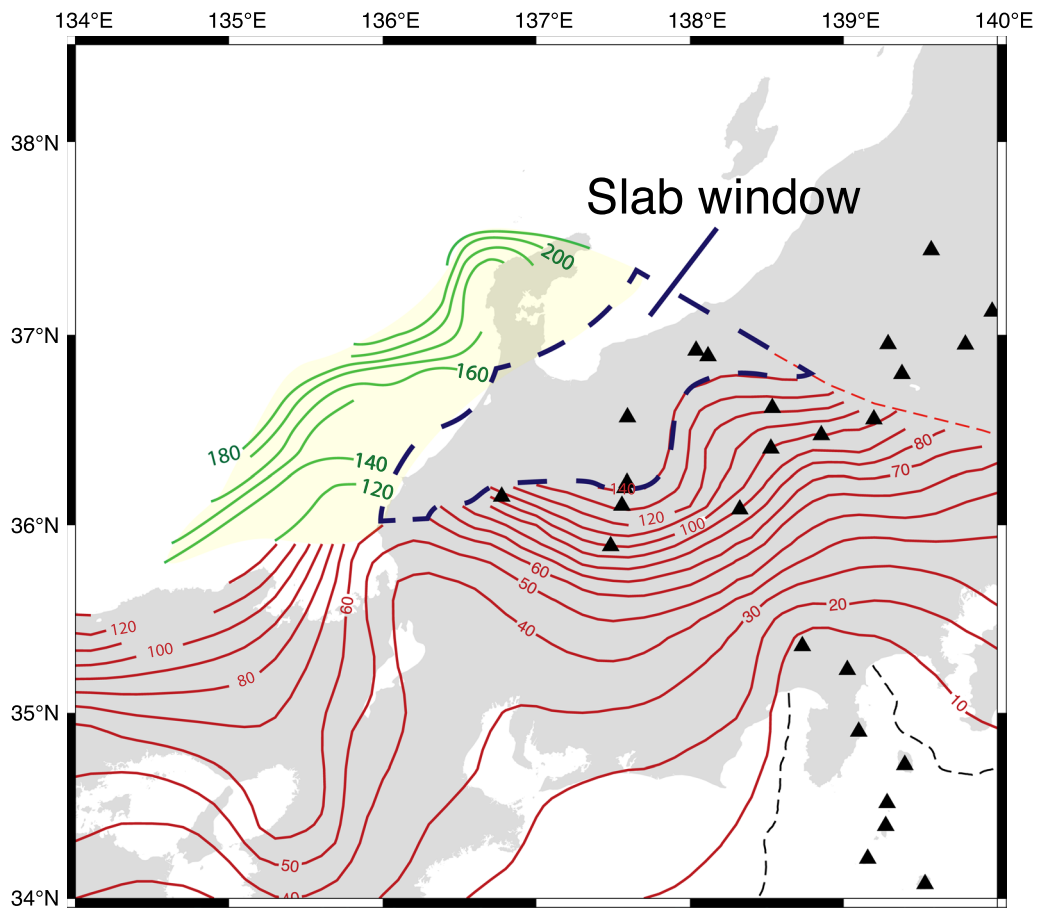
Fig. 7 Iso-depth contour map of the PHS slab geometry model obtained in this study. Red contours are from the existing PHS slab model. Green contours represent the upper surface of the PHS slab that has been estimated in this study. The area within the dashed blue line is the area where the PHS slab does not exist (i.e., slab window). The black triangles indicate volcanoes
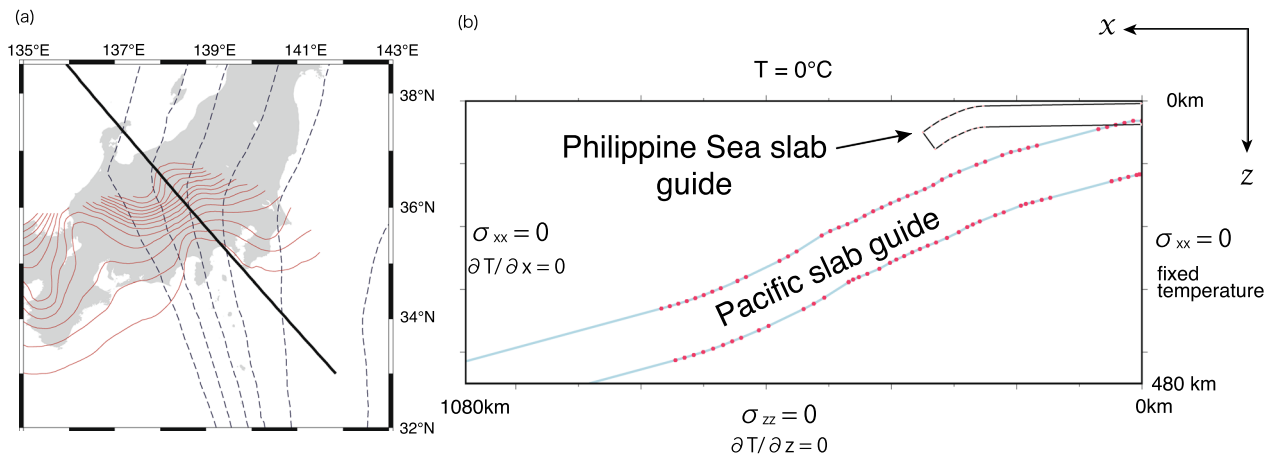

Fig. 8 Settings used for the numerical simulations. **a** Profile used in the numerical simulation. The shapes of the prescribed guides are calculated using the PHS slab (red lines) and PAC slab (dashed blue lines) model (Fig. 1). **b** Schematic figure of a 2D box-type thermal convection model. The dotted black line indicates the prescribed guide of the PHS slab used in the numerical simulation. The dotted light-blue line shows the guide of the PAC slab. The red dots indicate the positions of the intersection that control the dip angle of the PAC slab guide

Miyazaki *et al. Earth, Planets and Space* (2023) 75:93

Page 11 of 17

P_{lc} is lithostatic pressure, V is activation volume and R is the gas constant. The values of the model parameters used for the momentum equation, stream function and viscosity calculation are the same as those used in Yoshioka et al. (2015), but we ignore the viscosity change in the mantle transition zone because we focus on the subduction of the PHS slab at 50–250 km depth.

The momentum and energy equations were solved via a 2D finite-difference method. The size of the model domain was set to 1080 km horizontally and 480 km vertically (Fig. 8). The finite-difference grid spacing for the temperature and stream function calculations were set to 2.4 km and 12 km, respectively. We applied a normal stress of 0 Pa to the right, left and bottom boundaries, an isothermal condition of 0 °C to the model surface, an adiabatic condition to the left and bottom boundaries. For the right boundary, a time-dependent temperature-fixed condition was imposed, following Yoshioka and Sanshadokoro (2002):

$$Tz = T_0 \mathrm{erf}\left(\frac{z}{2\sqrt{\frac{kt_s}{\rho C_p}}} \right) \exp\left\{ \frac{\alpha g(z - z_s)}{C_p} \right\},$$

where $T(z)$ is the depth-dependent temperature, T_0 is the potential temperature, ρ is the density, t_s is the age of the oceanic plate at the trench, and z_s is the depth of the continental Moho (32 km). The exponential term represents the adiabatic compression, and the adiabatic compression is assumed to be included when $z > z_s$. The initial temperature structure in the continental plate is also calculated using the above equation, where t_s is determined as the apparent age of the continental plate, 5 Myr, to match the current average heat flow data on the continental side (Yoshioka et al. 2015).

We established guides along the subducting PHS and PAC plates, with the guide defining the geometry of the upper and lower boundaries of the subducting oceanic plate by kinematically imposing a stream function that corresponds to the subduction velocity. This allows the subduction of the oceanic plate to replicate the observed slab geometries. The thickness of the guides for the subducting plate was given by Yoshii (1975), which relates the thickness of the oceanic plates at the trench to their apparent ages. The initial age of the PAC plate was set to 100 Myr at the start of the subduction calculation, which yields a PAC plate thickness of 75 km, with the plate thickness (age) gradually increasing during the calculation. The age of the PHS plate was held constant at 25 Myr during the calculation, which corresponds to a plate thickness of ~ 40 km.

We considered a 2D profile that crosses the Noto peninsula (Fig. 8a) and simulated the subduction of the PAC

and PHS plates using the prescribed guides (Fig. 8b). This profile is parallel to the subduction direction of the PHS plate with respect to the North American plate in the MORVEL model (DeMets et al. 2010). The guide for the PAC plate was set for the entire model space, whereas the guide for the PHS plate was limited to 50 km depth to allow the PHS plate subduction to greater depths without any geometrical constraints (Fig. 8b). The subduction velocities of the PAC and PHS plates along the 2D profile were assumed to be 7.3 cm/yr and 3.9 cm/yr, respectively, based on the MORVEL model. We inserted the PHS plate into the calculation domain 5 Myr after subduction of PAC plate began.

Results

Figure 9 shows the results of temperature distribution for seven time steps after the initiation of the calculation (0 Myr), when subduction of the PAC plate began. The PHS plate is inserted into the model domain from the right boundary at 5 Myr (Fig. 9a) and moves on the surface until it starts to subduct at ~ 11 Myr (Fig. 9b). The leading edge of the PHS slab starts to extend beyond the guide at 13.2 Myr (Fig. 9c) and continues to subduct at a dip angle of ~ 30° (Fig. 9d, e). The leading edge of the PHS slab collides with the PAC slab at ~ 17 Myr (Fig. 9e), and the PHS slab is subsequently bent upward on the PAC slab (Fig. 9f). The leading edge of the PHS slab is completely separated from the main body of the PHS slab almost 3 Myr after its collision with the PAC slab, with this separated piece forming a "bump" on the upper surface of the PAC slab (the area enclosed by the dotted blue line in Fig. 9g). The bump remains emplaced on the upper surface of the PAC slab and is carried to greater depths as the PAC slab is subducted.

Bump formation

We performed the numerical simulation by changing several parameters. The results are shown in Additional file 1: Fig. S4. We note that the actual subductions of the PHS and PAC plates are 3D processes and that subduction direction of the two plates differ by ~ 20° (DeMets et al. 2010). Therefore, the subduction velocity of the plate is dependent on the direction of the calculated profile. Furthermore, it has been suggested that there were changes in the subduction direction and the velocity of the PHS plate at ~ 5 Ma, even though the subduction velocity of the PHS plate before 5 Ma is not well constrained (Seno and Maruyama 1984; Takahashi 2006; Kimura et al. 2014). Therefore, we conducted another numerical simulation that employed different PAC and PHS plate subduction velocities (Additional file 1: Fig. S4b–f). We also performed the numerical simulations using different plate ages to take investigate the
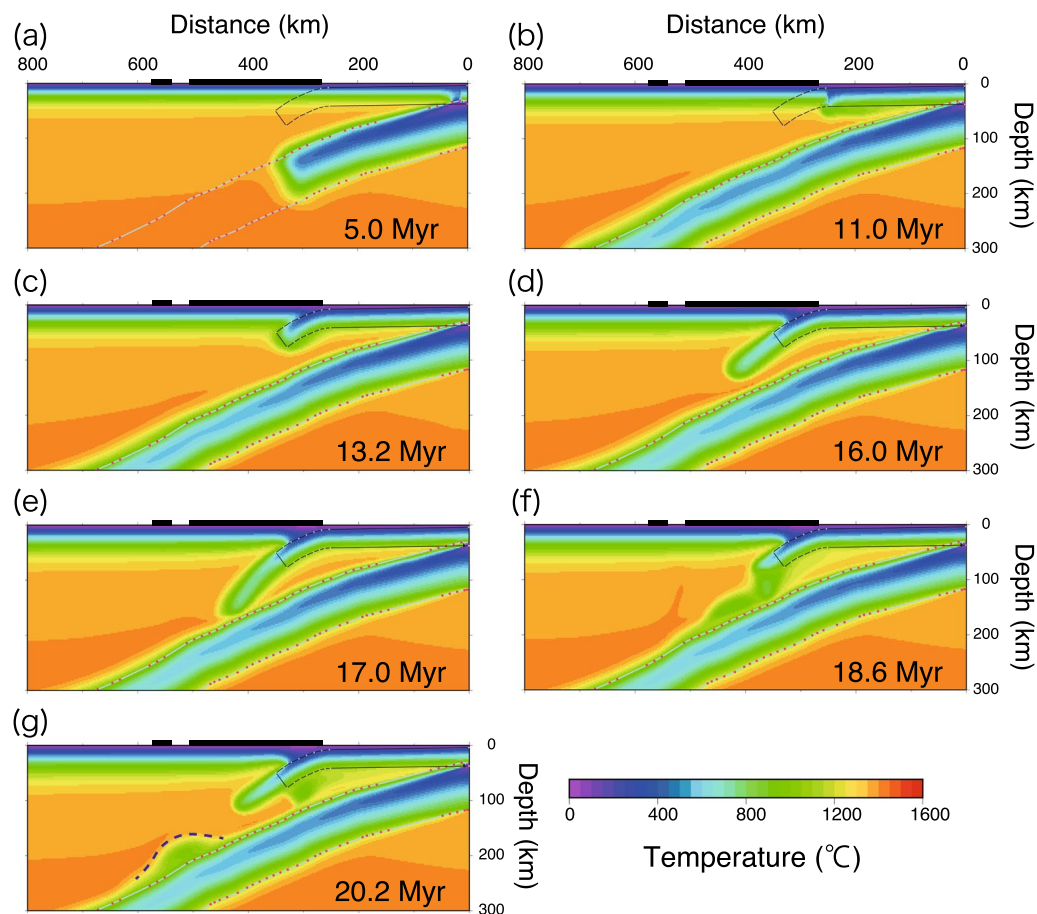
Fig. 9 Numerical simulation results. **a–g** Results at 5.0, 11.0, 13.2, 16.0, 17.0, 18.6, and 20.2 Myr from the initiation of the numerical simulation, respectively. Figures were drawn by cropping some of the computational domain. Dotted lines and red dots are the same as in Fig. 8b. Dashed lines in **g** represent the upper surfaces of the bump that formed owing to the collision between the PHS and PAC slabs. Black bars at the top of each figure represent the land areas

effect of the PHS plate thickness on its subduction history and geometry (Additional file 1: Fig. S4g).

We conducted additional numerical simulations for two 2D profiles that were shifted by about ± 50 km from the main profile to determinate the effect of the slab geometries on bump formation (Additional file 1: Fig. S5). All of the other parameters were the same as those along the main profile (Fig. 9). Although the PHS slab is subducted at gentler and steeper dip angles along these two profiles, the calculations still generate a bump along both profiles.

These various tests demonstrate that our numerical simulation results are robust and confirm that the bump formation is independent of the PHS and PAC plate subduction velocities, PHS plate age (thickness), and PAC and PHS slab geometry (dip angle). The temperature structure obtained in this study is similar to the 2D results from previous studies of the subducting PHS plate beneath Japan (Yoshioka et al. 2013, 2015) and the

2D cross section from regional 3D simulations (Yoshioka and Murakami 2007; Ji et al. 2016).

The numerical simulation results suggest that the lowermost PHS slab is torn from the shallow subducting PHS plate and becomes emplaced on the upper surface of the PAC slab when it collides with the underlying PAC slab. We attribute this separation along the subducting PHS slab to the difference in subduction velocities between the PAC and PHS plates. The faster subduction velocity of the PAC plate (7.3 cm/yr) compared with that of the PHS plate (3.9 cm/yr) likely forces the leading edge of the PHS slab to subduct at the same velocity as the PAC slab once it collides with the PAC slab. This process would likely generate a large tensional force in the PHS slab, resulting in the complete separation of the leading edge of the PHS slab from the main body.
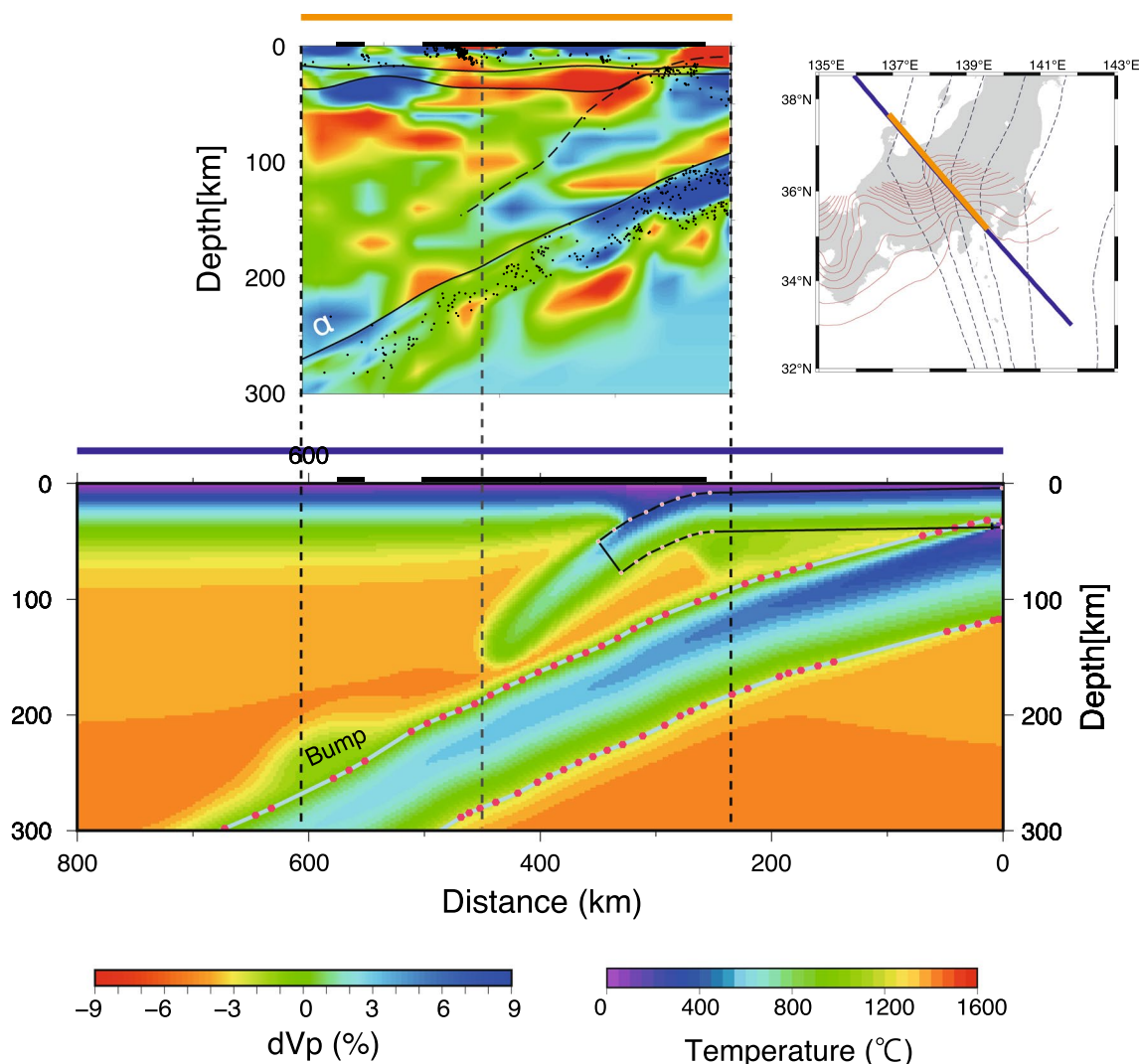
Miyazaki *et al. Earth, Planets and Space* (2023) 75:93

Page 13 of 17

Fig. 10 Comparison of tomographic (upper panel) and simulation (lower panel) results. Both results are along the same profile, with the tomography result fitted to the same *x*-axis as the simulation result; orange and blue lines on the map show the tomographic and simulation result locations, respectively. The dotted line represents the leading edge of the PHS slab used to compare the two results. The symbols in the figure are the same as in Fig. 4 for the tomography results and Fig. 9 for the simulation results

Discussion

There is a strong correlation between the inverted seismic velocity structure and simulated thermal structure results along the same profile (Fig. 10). Notably, the location and size of segment α located on the upper surface of the PAC slab beneath Noto peninsula are very similar to those of bump that formed on the upper surface of the PAC slab after the leading edge of the PHS slab collided with it. We therefore infer that segment α may have formed in response to the subducting PHS slab colliding with the PAC slab. We note, however, that these two different results cannot be compared on an absolute time scale owing to large uncertainties in the history of

movement of the PHS plate (Kimura et al. 2014), which are not introduced in our numerical simulation. We instead adjust the observed leading edge of the shallow subducting PHS slab in the relative sense to match that of the PHS slab in the numerical simulation results.

We performed the simulation along the profile that is parallel to the subduction direction of the PHS plate, but the subduction direction of the PAC plate is not parallel to it. We performed additional simulations with profiles E1 and E2 (Additional file 1: Fig. S6) to investigate the effect of the direction of profiles on the formation of the bump on the PAC slab. Profile E2 is parallel to the subduction direction of the PAC plate and passes through
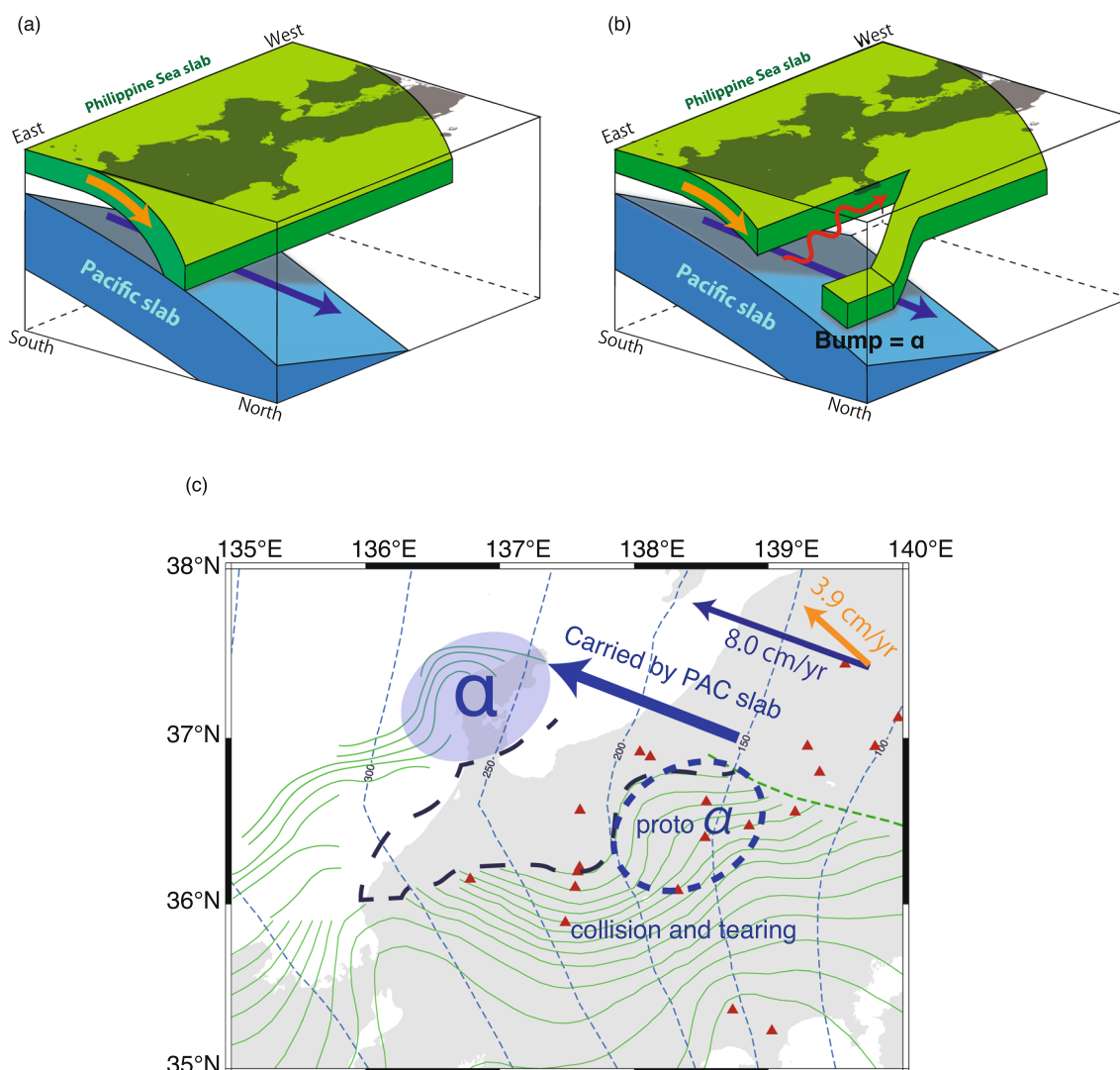
Fig. 11 A schematic figure of the evolution of the PHS slab beneath central Japan. **a** The leading edge of the subducting PHS slab (green) first collides the PAC slab (blue) in the east. **b** The PHS slab tears in the subduction direction after the collision, and the tear propagates westward (red arrows). Segment α (= bump) of the PHS slab beneath the Noto peninsula is only continuous in the southwest–northeast direction, forming a triangular slab window beneath the Hokuriku region. **c** Showing **b** on a map. Currently, segment α (= bump) is located beneath Noto peninsula. The red triangles indicate the volcanoes

the segment α. Profile E1 passes through the segment α and has an azimuth bisecting profile E2 and the profile used in the main simulation (Fig. 8). As a result, a bump forms in both simulations (Additional file 1: Fig. S6a, b), and we confirmed that the bump formation is robust regardless of the direction of calculation profiles.

The gradual westward deepening of the PAC slab at a dip angle of $\sim 30°$ (Fig. 1) indicates that the PHS slab first collided with the PAC slab in the easternmost part of the central Japan, where the depth of the PAC slab is the shallowest. Therefore, the tearing of the PHS slab

likely initiated along its easternmost edge (Fig. 11a). In this framework, the easternmost of the PHS slab was isolated as a bump, then carried by the PAC slab toward its subduction direction, and currently exists as segment α beneath the Noto peninsula (Fig. 11c). The tensional forces that were generated by the differences in the PHS and PAC plate subduction velocities potentially facilitated westward tearing of the PHS slab over time (Fig. 11b). Conversely, the subducting PHS slab in the western part of the central Japan has not yet come in contact with the PAC slab, such that the above-mentioned

Miyazaki *et al. Earth, Planets and Space* (2023) 75:93

Page 15 of 17

tensional forces gradually decrease to the west along the subducting PHS slab. This process may have resulted in the formation of a triangular slab window that opens to the east, as delineated by the seismic tomography results (Fig. 7).

The existence of slab tear has been observed in the Mediterranean (Wortel and Spakman 2000). It has been proposed that the slab tear in this region is driven mainly by the tensile forces owing to the positive buoyancy of the continental lithosphere and negative buoyancy of the subducting slab, resulting in the tear propagating in a direction perpendicular to the subduction (Yoshioka and Wortel 1995; Faccenna et al. 2006; van Hunen and Allen 2011). Although the Mediterranean and central Japan have different tectonic frameworks, both slab tears are suggested to have occurred in response to tensional forces that formed within the subducting slab. These results suggest that the subducting slab can be easily deformed and torn, even though it is considered to be a rigid body, when internal forces that are larger than the mechanical strength of the slab are applied.

Conclusion

We performed two independent analyses, seismic tomography and a numerical simulation of two subducting plates, to investigate the tectonics of the PHS plate subducting beneath central Japan. The seismic tomography results revealed continuous subduction of the PHS plate, with the subducted plate extending from beneath Wakasa bay to beneath the Noto peninsula and reaching a maximum depth of ~ 250 km beneath Hokuriku region, which is > 50 km deeper than that in previous models of the PHS plate subduction in this region. Our tomography results also revealed an area with no PHS slab beneath the Hokuriku region, thereby forming a broad triangular slab window that tapers to the west. The numerical simulation indicated that the PHS plate had collided with the PAC plate, with the once leading edge of the PHS slab tearing from the main plate body owing to the difference in subduction velocities between the two plates. A combined interpretation of the seismic tomography and numerical simulation results suggests that the observed slab tear is generated by the frictional interactions between the PHS slab and the underlying PAC slab. Further studies would include 3D simulations to investigate the three-dimensional process of the dual plate subduction and the formation of the tear of the PHS slab beneath central Japan.

Abbreviations

PHS   Philippine Sea
PAC   Pacific
KPR   Kyushu–Palau Ridge
IBM   Izu–Bonin Mariana
JMA   Japan Meteorological Agency
CRT   Checkerboard Resolution Tests
2D   Two-dimensional
3D   Three-dimensional

Supplementary Information

The online version contains supplementary material available at https://doi.org/10.1186/s40623-023-01846-z.

Additional file 1. Fig. S1: Depth slices of the checkerboard test results. Shaded areas in the figuresrepresent the subducting PAC plate. **Fig. S2**: Depth slices of the tomographic results. Areas that are sampled by < 1000 rays are shown in white. **Fig. S3**: Vertical cross section of the tomography results performed by changing some of the parameters. All of the results are along profile B1. See Additional file 1: Table S1 for the detailed parameters. **Fig. S4**: Results of the numerical simulations performed using different parameters. It is noted that the timing of collision varies depending on the subduction velocities of the two plates; therefore, the time is not identical for each figure. See Additional file 1: Table S2 for the detailed parameters. **Fig. S5**: Results of the numerical simulation that were performed by shifting the calculated profiles about ± 50 km. Each detailed profile is shown in the map. The thick dashed black line in the map indicates the profile used in the main result. **Fig. S6**: Results of additional numerical simulation. Profile E2 is parallel to the direction of the PAC plate subduction and crosses the segment α. Profile E1 crosses the segment α and has a bisecting azimuth between profile E2 and the profile used in the main simulation. Blue dotted line inandindicate bump. The map shows profiles overlaid on the result of seismic tomography at depth of 240 km in this study. **Table S1**: Parameter values for the results in Additional file 1: Fig. S3. **Table S2**: Parameter values for the results in Fig. S4.

Author contributions

KM and JN designed the research plan, and KM performed tomographic inversions and numerical simulations. All authors read and approved the final manuscript.

Availability of data and materials

The final P-wave velocity model obtained by seismic tomography and simulation results obtained by numerical simulation shown in Fig. 9 can be accessed at https://doi.org/10.5281/zenodo.7907062. Travel-time data set used in this study can be accessed at the same address, but these can be used only for validation and evaluation of the conclusions described in the manuscript. Please refrain conducting new research using this data set. Original Arrival-time data set is available at the JMA (https://www.data.jma.go.jp/svd/eqev/data/bulletin/deck_e.html).

Declarations

Ethics approval and consent to participate

Not applicable.

Author details
[1]Department of Earth and Planetary Science, School of Science, Tokyo Institute of Technology, Tokyo, Japan. [2]Research Center for Urban Safety and Security, Kobe University, Kobe, Japan. [3]Faculty of Science, Graduate School of Science, Kobe University, Kobe, Japan.

References
Abdelwahed MF, Zhao D (2007) Deep structure of the Japan subduction zone. Phys Earth Planet Inter 162:32–52

Arai R, Iwasaki T, Sato H, Abe S, Hirata N (2014) Contrasting subduction structures within the Philippine Sea plate: hydrous oceanic crust and anhydrous volcanic arc crust. Geochem Geophys Geosyst 15:1977–1990

Asamori K, Zhao D (2015) Teleseismic shear wave tomography of the Japan subduction zone. Geophys J Int 203:1752–1772

Burkett ER, Billen MI (2010) Three-dimensionality of slab detachment due to ridge-trench collision: laterally simultaneous boudinage versus tear propagation. Geochem Geophys Geosyst 11:Q11012

Cao L, Wang Z, Wu S, Gao X (2014) A new model of slab tear of the subducting Philippine Sea plate associated with Kyushu–Palau Ridge subduction. Tectonophys 636:158–169

DeMets C, Gordon RG, Argus DF (2010) Geologically current plate motions. Geophys J Int 181:1–80

Faccenna C, Bellier O, Martinod J, Piromallo C, Regard V (2006) Slab detachment beneath eastern Anatolia: a possible cause for the formation of the North Anatolian fault. Earth Planet Sci Lett 242:85–97

Hasegawa A, Nakajima J, Kita S, Okada T, Matsuzawa T, Kirby SH (2007) Anomalous deepening of a belt of intraslab earthquakes in the Pacific slab crust under Kanto, central Japan: possible anomalous thermal shielding, dehydration reactions, and seismicity caused by shallower cold slab material. Geophys Res Lett 34:L09305

Hirose F, Nakajima J, Hasegawa A (2008) Three-dimensional seismic velocity structure and configuration of the Philippine Sea slab in southwestern Japan estimated by double-difference tomography. J Geophys Res Solid Earth 113:B09315

Hua Y, Zhao D, Xu Y, Liu X (2018) Age of the subducting Philippine Sea slab and mechanism of low-frequency earthquakes. Geophys Res Lett 45:2303–2310

Huang Z, Zhao D, Hasegawa A, Umino N, Park JH, Kang IB (2013) Aseismic deep subduction of the Philippine Sea plate and slab window. J Asian Earth Sci 75:82–94

Ide S, Shiomi K, Mochizuk K, Tonegawa T, Kimura G (2010) Split Philippine sea plate beneath Japan. Geophys Res Lett 37:L21304

Ishida M (1992) Geometry and relative motion of the Philippine Sea plate and Pacific plate beneath the Kanto-Tokai district, Japan. J Geophys Res Solid Earth 97:489–513

Ishise M, Miyake H, Koketsu K (2015) Dual subduction tectonics and plate dynamics of central Japan shown by three-dimensional P-wave anisotropic structure. Phys Earth Planet Inter 244:49–68

Iwamori H (2000) Deep subduction of H2O and deflection of volcanic chain towards backarc near triple junction due to lower temperature. Earth Planet Sci Lett 181:41–46

Ji Y, Yoshioka S, Matsumoto T (2016) Three-dimensional numerical modeling of temperature and mantle flow fields associated with subduction of the Philippine Sea plate, southwest Japan. J Geophys Res Solid Earth 121:4458–4482

Katsumata A (2010) Depth of the Moho discontinuity beneath the Japanese islands estimated by traveltime analysis. J Geophys Res Solid Earth 115:B04303

Kimura G, Hashimoto Y, Kitamura Y, Yamaguchi A, Koge H (2014) Middle Miocene swift migration of the TTT triple junction and rapid crustal growth in southwest Japan: a review. Tectonics 33:1219–1238

Kono A, Sato T, Shinohara M, Mochizuki K, Yamada T, Uehira K, Shinbo T, Machida Y, Hino R, Azuma R (2017) Geometry and spatial variations of seismic reflection intensity of the upper surface of the Philippine Sea plate off the Boso Peninsula, Japan. Tectonophysics 709:44–54

Liu X, Zhao D (2016) P and S wave tomography of Japan subduction zone from joint inversions of local and teleseismic travel times and surface-wave data. Phys Earth Planet Inter 252:1–22

Nakahigashi K, Shinohara M, Yamada T, Uehira K, Sakai S, Mochizuki K, Shiobara H, Kanazawa T (2015) Deep slab dehydration and large-scale upwelling flow in the upper mantle beneath the Japan Sea. J Geophys Res Solid Earth 120:3278–3292

Nakajima J (2018) Isolated intermediate-depth seismicity north of the Izu peninsula, Japan: implications for subduction of the Philippine Sea Plate. Earth Planets Space 70:1–10. https://doi.org/10.1186/s40623-018-0779-7

Nakajima J (2019) Revisiting intraslab earthquakes beneath Kyushu, Japan: effect of ridge subduction on seismogenesis. J Geophys Res Solid Earth 124:8660–8678

Nakajima J, Hasegawa A (2006) Anomalous low-velocity zone and linear alignment of seismicity along it in the subducted Pacific slab beneath Kanto, Japan: Reactivation of subducted fracture zone? Geophys Res Lett 33:L16309

Nakajima J, Hasegawa A (2007) Subduction of the Philippine Sea plate beneath southwestern Japan: slab geometry and its relationship to arc magmatism. J Geophys Res Solid Earth 112:B08306

Nakajima J, Hirose F, Hasegawa A (2009) Seismotectonics beneath the Tokyo metropolitan area, Japan: effect of slab-slab contact and overlap on seismicity. J Geophys Res Solid Earth 114:B08309

Nakamura H, Iwamori H, Kimura JI (2008) Geochemical evidence for enhanced fluid flux due to overlapping subducting plates. Nat Geosci 1:380–384

Okino K, Shimakawa Y, Nagaoka S (1994) Evolution of the Shikoku basin. J Geomagn Geoelect 46:463–479

Park JO, Hori T, Kaneda Y (2009) Seismotectonic implications of the Kyushu–Palau ridge subducting beneath the westernmost Nankai forearc. Earth Planets Space 61:1013–1018. https://doi.org/10.1186/BF03352951

Sano Y, Nakajima J (2008) Geographical distribution of 3He/4He ratios and seismic tomography in Japan. Geochem J 42:51–60

Sano Y, Kameda A, Takahata N, Yamamoto J, Nakajima J (2009) Tracing extinct spreading center in SW Japan by helium-3 emanation. Chem Geol 266:50–56

Sekiguchi S (2001) A new configuration and an aseismic slab of the descending Philippine Sea plate revealed by seismic tomography. Tectonophys 341:19–32

Sdrolias M, Roest WR, Müller RD (2004) An expression of Philippine Sea plate rotation: the Parece Vela and Shikoku basins. Tectonophys 394:69–86

Seno T, Maruyama S (1984) Paleogeographic reconstruction and origin of the Philippine Sea. Tectonophys 102:53–84

Takahashi M (2006) Tectonic development of the Japanese Islands controlled by Philippine Sea Plate motion (in Japanese with English abstract). J Geogr 115:116–123

Torii Y, Yoshioka S (2007) Physical conditions producing slab stagnation: Constraints of the Clapeyron slope, mantle viscosity, trench retreat, and dip angles. Tectonophys 445:200–209

Uchida N, Nakajima J, Hasegawa A, Matsuzawa T (2009) What controls interplate coupling? Evidence for abrupt change in coupling across a border between two overlying plates in the NE Japan subduction zone. Earth Planet Sci Lett 283:111–121

Uchida N, Matsuzawa T, Nakajima J, Hasegawa A (2010) Subduction of a wedge-shaped Philippine Sea plate beneath Kanto, central Japan, estimated from converted waves and small repeating earthquakes. J Geophys Res Solid Earth 115:B07309

Ueno H (2002) Improvement of hypocenter determination procedures in the Japan Meteorological Agency (in Japanese with English abstract). QJ Seismol 65:123–134

van Hunen J, Allen MB (2011) Continental collision and slab break-off: a comparison of 3-D numerical models with observations. Earth Planet Sci Lett 302:27–37

Wada I, He J (2017) Thermal structure of the Kanto region, Japan. Geophys Res Lett 44:7194–7202

Wang J, Zhao D (2012) P wave anisotropic tomography of the Nankai subduction zone in Southwest Japan. Geochem Geophys Geosyst 13:Q05017

Wortel MJR, Spakman W (2000) Subduction and slab detachment in the Mediterranean-Carpathian region. Science 290:1910–1917

Yamamoto S, Nakajima J, Hasegawa A, Maruyama S (2009) Izu–Bonin arc subduction under the Honshu island, Japan: evidence from geological and seismological aspect. Gondwana Res 16:572–580

Yamamoto Y, Obana K, Takahashi T, Nakanishi A, Kodaira S, Kaneda Y (2013) Imaging of the subducted Kyushu–Palau Ridge in the Hyuganada region, western Nankai Trough subduction zone. Tectonophys 589:90–102

Yoshii T (1975) Regionality of group velocities of Rayleigh waves in the Pacific and thickening of the plate. Earth Planet Sci Lett 25:305–312

Yoshioka S, Murakami K (2007) Temperature distribution of the upper surface of the subducted Philippine Sea Plate along the Nankai Trough, southwest Japan, from a three-dimensional subduction model: relation to large interplate and low-frequency earthquakes. Geophys J Int 171:302–315

Yoshioka S, Sanshadokoro H (2002) Numerical simulations of deformation and dynamics of horizontally lying slabs. Geophys J Int 151:69–82

Yoshioka S, Wortel MJR (1995) Three-dimensional numerical modeling of detachment of subducted lithosphere. J Geophys Res Solid Earth 100:20223–20244

Yoshioka S, Suminokura Y, Matsumoto T, Nakajima J (2013) Two-dimensional thermal modeling of subduction of the Philippine Sea plate beneath southwest Japan. Tectonophys 608:1094–1108

Yoshioka S, Takagi R, Matsumoto T (2015) Relationship between temperatures and fault slips on the upper surface of the subducting Philippine Sea plate beneath the Kanto district, central Japan. Geophys J Int 201:878–890

Zhao D, Hasegawa A, Horiuchi S (1992) Tomographic imaging of P and S wave velocity structure beneath northeastern Japan. J Geophys Res Solid Earth 97:19909–19928

Zhao D, Yanada T, Hasegawa A, Umino N, Wei W (2012) Imaging the subducting slabs and mantle upwelling under the Japan Islands. Geophys J Int 190:816–828

Publisher's Note